A Simulation Study of the Landfall of Tropical Cyclones Using a Movable Nested-Mesh Model

ROBERT E. TULEYA, MORRIS A. BENDER AND YOSHIO KURIHARA

Geophysical Fluid Dynamics Laboratory/NOAA, Princeton University, Princeton, NJ 08540

(Manuscript received 1 April 1983, in final form 26 August 1983)

ABSTRACT

By use of a triply nested, movable mesh model, several ideal simulations of tropical cyclone landfall were performed for a strong zonal flow of ~10 m s^{-1}. The integration domain was a 37 × 45° channel with the innermost mesh having a 22 × 22 point resolution of ½°. General characteristics similar to observed landfalling tropical cyclones are obtained in the primary simulation experiment including an abrupt change in the low level (~68 m) winds at the coastline and a decay of the tropical cyclone as it moves inland. Additional interesting features subject to model and experimental limitations include: little noticeable track change of the model storm when compared to a control experiment with an ocean surface only; a possible temporary displacement of the center of the surface wind circulation from the surface pressure center at landfall; and a distinct decrease in kinetic energy generation and precipitation a few hours after landfall.

The sensitivity to the specified land surface conditions was analyzed by performing additional experiments in which the land surface conditions including surface temperature, moisture, and distribution of surface roughness were changed. It was found that a reasonable change in some of these land conditions can make a considerable difference in behavior for a landfalling tropical cyclone. It was also shown that a small, less intense model storm fills less rapidly. This corresponds well with observations that many landfalling hurricanes decay to approximately the same asymptotic value one day after landfall.

1. Introduction

The analysis of landfalling tropical cyclones is obviously of great interest both pragmatically and scientifically. Until recently landfalling tropical cyclones have not been analyzed extensively because the mesoscale structure of these storms cannot be resolved by the standard synoptic observation network, and upper air data from aircraft are often unavailable over land. Early observational research has been accomplished by Hubert (1955), Miller (1964), Brunt (1968) and others. Recent studies include those of Fujita (1980), Powell (1982) and Parrish *et al.* (1982). These give detailed case study analyses of surface wind and rainfall characteristics at landfall.

Development of numerical models of landfalling storms has also been slow. Operational primitive equation models are used primarily for storm track prediction, not intensity. To simulate boundary layer changes and related mesoscale structural changes at landfall, a sophisticated model with both fine resolution in the vertical and horizontal is required. The real data requirements on a fine scale, limited domain present numerous observational and numerical problems. In spite of these difficulties, model simulations of ideal landfalling storms have been performed by Tuleya and Kurihara (1978), Moss and Jones (1978) and Chang (1982).

The major decay mechanism in landfalling tropical cyclones is the virtual elimination of surface evaporation as determined from the aforementioned studies and summarized by Simpson and Riehl (1981) and Anthes (1982). These studies have shown that the increased land surface roughness affects the boundary layer wind structure, but the storm as a whole will not significantly decay unless the evaporation is suppressed. In the earlier numerical study of Tuleya and Kurihara (1978, hereafter referred to as TK), a simplified experimental scheme was used in which the storm was fixed in the computational domain and the land-sea boundary moved through the domain at a speed of 10 m s^{-1}. The evaporation was cut off over the land *a priori* and no beta effect nor explicit steering current was included in the model. In the present study a basic flow of 10 m s^{-1} and the variation of the Coriolis parameter were explicitly included.

The aim of this study is to investigate the phenomena of landfall using a more sophisticated model than used previously but with a still simple experimental framework, in order to isolate decay mechanisms and landfall behavior. This is nearly impossible from observational analyses or from a real data simulation case study. Given the realistic nature of the primary simulation, the sensitivity of the landfall phenomena to changes of surface conditions will be investigated. Landfall experiments will also be performed with two distinct

storm sizes with the difference in behavior discussed. The model results will also be compared with observation, especially the key parameter of decay rate, rainfall and low level wind patterns. In making these comparisons, one must remember that the model results are for landfall under idealized conditions, such as a uniform easterly steering current, fixed land and ocean surface temperatures, no topography, and no interaction with continental air masses. In reality, the direction and speed of the steering current, land and ocean temperatures and topography vary from one case to another. These parameters and their differences from one case to another and from this particular simulation model have an effect on the precipitation and wind patterns at landfall. The extent of this effect remains to be investigated. In addition, one may be forced to compare two quantities that are not quite the same; e.g., average composited data compared with instantaneous model results, or estimated gusts at one height with mean model winds valid at a slightly different height. These differences must be kept in mind when comparing model and observed results.

A description of the experimental design including the model grid system and the initialization and specification of the various experiments are found in Section 2. A detailed analysis of the low level winds, precipitation, and moisture and energy budgets of the primary experiment are described in Section 3. Section 4 contains a comparative analysis of the effects of different land surface conditions on the decay process. In Section 5 the effect of storm intensity on the filling rates of both model and observed storms is discussed. A summary of the results and conclusions is presented in Section 6.

2. Experimental design

The experimental strategy of the model design, initialization and specifications for the various experiments are explained in this section. The more relevant features of the model design and physical specifications are emphasized.

a. Model used

For this study, the triply nested, movable grid system described by Kurihara and Bender (1980) is utilized. The integration domain is a 37° latitude (5.5° to 42.5°N) × 45° longitude area with the innermost nest consisting of a 22 × 22 point uniform mesh of ⅙° resolution. Some specific mesh parameters are summarized in Table 1. The model used is an eleven level primitive equations model (Kurihara and Bender, 1980) formulated in longitude, latitude, sigma coordinates. Some of the relevant characteristics of the model include a Monin-Obukhov framework for the interactions at the surface, a vertical mixing scheme described by Mellor and Yamada (1974), and cumulus

TABLE 1. Grid system of the triply nested-mesh model used in the landfall experiments.

Mesh	Grid resolution (deg)	Time step (s)	Domain size: Longitude (points)	Domain size: Latitude (points)
1	1	150	45° (45)	37° (37)
2	⅓	50	11° (33)	11° (33)
3	⅙	25	3⅔° (22)	3⅔° (22)

parameterization described by Kurihara (1973). At the surface, the downward flux of momentum τ, the upward sensible heat flux H and the water vapor flux E are computed from the following formulas:

$$\left.\begin{aligned} \tau &= \rho \mathbf{V}_*^2 \frac{\mathbf{V}(h)}{|\mathbf{V}(h)|} \\ H &= \rho C_p |\mathbf{V}_*| \theta_* \\ E &= \rho |\mathbf{V}_*| r_* \end{aligned}\right\}, \tag{2.1}$$

where ρ is the density of air, C_p the specific heat at constant pressure, $\mathbf{V}_*$ the frictional velocity, θ_* the frictional potential temperature, r_* the frictional mixing ratio, and $\mathbf{V}(h)$ the vector wind at height h. The top of the constant flux layer h is assumed to extend up to the lowest model level ($\sigma = 0.992$, ~68 m). The frictional values ($\mathbf{V}_*$, θ_*, r_*) are obtained iteratively when: $\mathbf{V}$, θ, and r are given at h; θ and r at the surface are specified; and z_0 is either calculated by Charnock's relation over the ocean or specified over the land (for more details, see Kurihara and Tuleya, 1974, p. 897). The surface values $\theta(o)$ and $r(o)$ may be changed from sea to land conditions. The quantity $r(o)$ can be formulated as:

$$r(o) = \left.\begin{aligned} r_{\mathrm{SAT}} w &\quad \text{for land} \\ r_{\mathrm{SAT}} &\quad \text{for ocean} \end{aligned}\right\}, \tag{2.2}$$

where r_{SAT} is the saturation mixing ratio at the surface temperature, and w is a moisture availability coefficient for the land. In the present study w is set to either 0.0 or 1.0, and $\theta(o)$ is specified as either 298 or 302 K over the land and 302 K over the ocean.

The model is initialized with the superposition of a vortex centered at 22°N on a zonal flow of constant angular velocity with easterlies of 10 m s^{-1} at 20°N. This relatively large zonal flow was selected to match the implied 10 m s^{-1} storm movement of TK. The initial vortex is prescribed in similar fashion as in Kurihara and Bender (1982) with the boundary layer flow

$$V(R) = V_m \frac{2R}{R_m}\left[1 + \left(\frac{R}{R_m}\right)^3\right]^{-1} \frac{R_0 - R}{R_0}, \tag{2.3}$$

where V is the wind magnitude, R the radius from the

center, and V_m, R_m, and R_0 are specified as 12 m s^{-1}, 200 km, and ∞, respectively. Such a specification makes a storm size and strength in the present model similar to those of TK if the part of the wind field due to the zonal flow is accounted for. The mass field is obtained from the reverse balance equation in the nested framework as described by Kurihara and Bender (1980).

b. *Specification of land conditions*

Given the aforementioned initialization, the weak vortex over the ocean is allowed to intensify into hurricane strength. The model is integrated to ~55 h with cyclic conditions at the eastern and western boundaries and with an open boundary condition, described by Kurihara and Bender (1983), at the northern and southern boundaries. At ~55 h, the land surface conditions are implemented at all latitudes for a 23° longitudinal span in the western part of the computational domain 8° west of the storm center. The cyclic boundary conditions are then replaced by the open boundary condition. In this scheme flow normal to the boundary is damped toward a specified value for both inflow and outflow, and flow tangent to the boundary is damped toward a specified value for inflow and extrapolated for outflow conditions. Landfall occurs in most simulations at ~77 h, and the simulations extend to 96 h. An ocean-only control experiment is also utilized for comparison purposes.

In the primary landfall experiment, a moist land (i.e., w = 1.0) with a land surface temperature (LST) of 298 K and roughness parameter, z_0, of 25 cm are specified. Because of the cool LST and the relatively warm moist boundary layer of the landfalling storm, it can be anticipated that the evaporation will initially be considerably reduced despite the moist land. In other supplementary experiments, either the land surface temperature is specified as 302 K, the evaporation is totally precluded (i.e., w = 0.0), or the roughness parameter is varied irregularly from 10 cm at the coastline to a maximum of 100 cm inland. In Table 2, the features of the experiments performed and their designated names are listed.

3. Landfall simulation

As previously stated, LST was set to 298 K, w = 1.0, and z_0 = 25 cm in the primary landfall experiment. The vortex was initialized with R_m = 200 km and R_0 = ∞ in (2.3) with the simulation designated as experiment L298. A cool land surface temperature was specified to simulate conditions under the cloud canopy of the storm—the surface temperature being cooled by evaporation and lack of solar insolation. Miller (1964) has indicated that surface temperatures in Hurricane Donna, 1960, were about 2–4 K lower over the land than over the ocean. This experiment was studied in detail because it mitigated the rather severe limitations of previous numerical studies of landfall and demonstrated the capability of the movable nested-mesh model in simulating landfall.

a. *Time history of maximum low level winds*

The disturbance reached maximum intensity (i.e., minimum central surface pressure) ~1 h prior to landfall and filled 14 mb in the first 6 h after landfall. Landfall, the time when the central pressure minimum encountered land, occurred at 76.3 h. By 81 h the low level winds had subsided to below hurricane force. Fig. 1 shows the swath of maximum low level winds (at σ = 0.992) for both the experiment L298 and the ocean-only control case. Notice the near discontinuity at the coastline as has been observed by Powell (1982) and the rapid decrease in the area of maximum winds of hurricane force (>33 m s^{-1}, shaded area). In this experiment the hurricane force winds penetrated ~165 km inland. This can be compared to the penetration of ~132 and ~230 km of estimated surface gusts for Hurricane Camille in 1969 and Frederic in 1979, respectively, as reported by Fujita (1980), although both of these observed storms moved north and normal to the coast at a forward speed of 7 m s^{-1} at landfall. It will be shown later that this decay rate is a function of the land surface conditions specified in the model. Fig. 1 shows that in the landfalling storm there was no major deflection in the storm track at landfall. At 84 h the landfalling storm was only ~20 km to the right and behind the position of the ocean control case

TABLE 2. Specification of land surface temperature (LST), moisture availability (w), roughness length over the land (z_0) and the size parameters [R_m and R_0 in (2.3)] of the initial vortex. Sea surface temperature is fixed at 302 K in all experiments.

Experiment	LST (K)	w	z_0 (cm)	R_m (km)	R_0 (km)	Main feature
Control	—	—	—	200	∞	All ocean (no land)
L298 (primary experiment)	298	1.0	25	200	∞	Low LST, moist land
L302	302	0.0	25	200	∞	High LST, no land moisture
V298	298	1.0	10–100	200	∞	Nonhomogeneous z_0
S302	302	0.0	25	150	1667	Small vortex, no land moisture

storm. At 90 h this difference increased to ~50 km as the storm decayed.

b. Low level wind analyses at landfall

Synoptic analyses of the low level wind field at 73, 77, 81 and 89 h are presented in Fig. 2. Just after landfall, the distortion of the wind isopleths is evident with two distinct maximum wind areas and an abrupt discontinuity along the coast. The low level wind distribution at the coastline results in convergence and divergence bands at the onshore and offshore flow side, respectively, of the point of landfall as has been described by TK for a model simulation and by Powell (1982) for Frederic in 1979. Also at landfall (Fig. 2, upper right) there is a slight tendency (10 km) for the center of the surface wind circulation to lag the surface pressure center which is denoted by the hurricane symbol. The displacement of the eye and surface pressure center was observed in the supplementary experiments

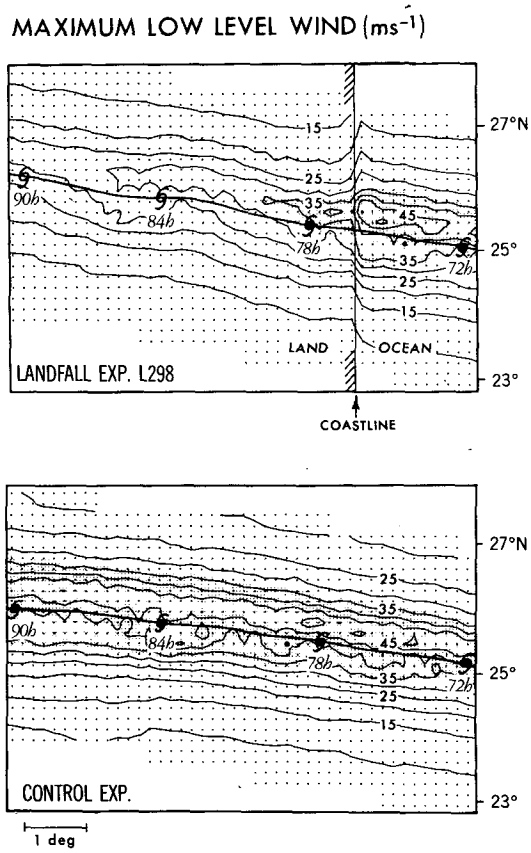

FIG. 1. Horizontal distribution of maximum low level (σ = 0.992) wind during the tropical storm passage for the basic landfall experiment, L298 (upper) and for the ocean-only experiment (lower). Storm tracks are shown with 6 h positions indicated. Shading indicates hurricane force winds (>33 m s^{-1}). Land is to the west of the indicated coastline, and the dots indicate the fine mesh resolution of ~17 km at 25°N.

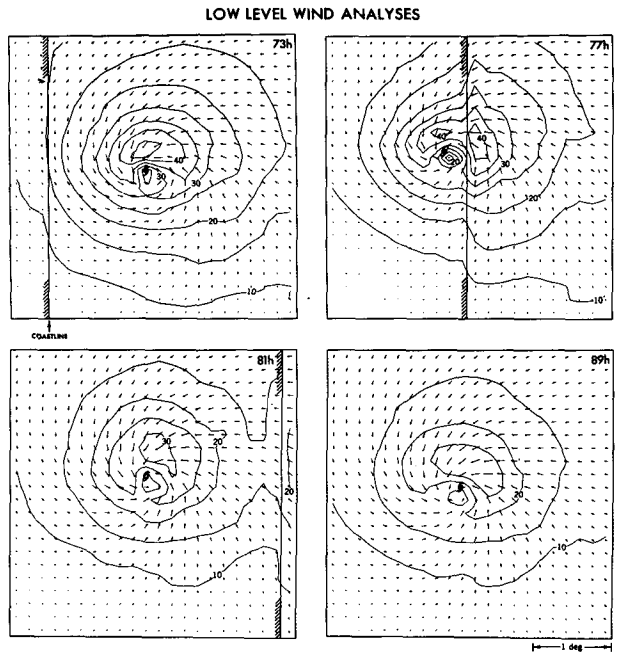

FIG. 2. Low level (σ = 0.992) wind analyses for the basic landfall experiment, L298, for 73, 81 and 89 h. The center of the storm as defined by the surface pressure field is indicated by the hurricane or tropical storm symbol. Isotachs (m s^{-1}) and vectors indicate wind magnitude and direction, respectively. Land is to the west of the indicated coastline.

and there were indications of this in Frederic as well.[1] At 77 h, the maximum low level winds have decreased to less than 45 m s^{-1} and by 81 h the low level winds are below hurricane intensity. Another interesting feature is the tendency for the time mean position of maximum low level winds to shift from right front quadrant of the storm over water to right rear quadrant over land. Although Fig. 2 is valid at the four specified instantaneous times, the change in the pattern of isotachs from that of 73 h to those at 81 and 89 h exemplifies the above mentioned shift. The right front position of the maximum winds over ocean was observed in the composite analysis of Shea and Gray (1973) and in Frederic, 1979, by Powell (1982). However, it is found in the present study that the location of the maximum winds fluctuates considerably around a time mean position and even in the ocean control case the maximum surface winds appear in the right rear quadrant ~36% of the time between 71 and 92 h.

One can take a closer look at the time history of the low-level wind field at the grid points near the point of landfall (Fig. 3). At the two grid points immediately to the left of the storm track there is an

[1] Personal communication with M. Powell of the Atlantic Oceanographic and Meteorological Laboratory, February 1983.

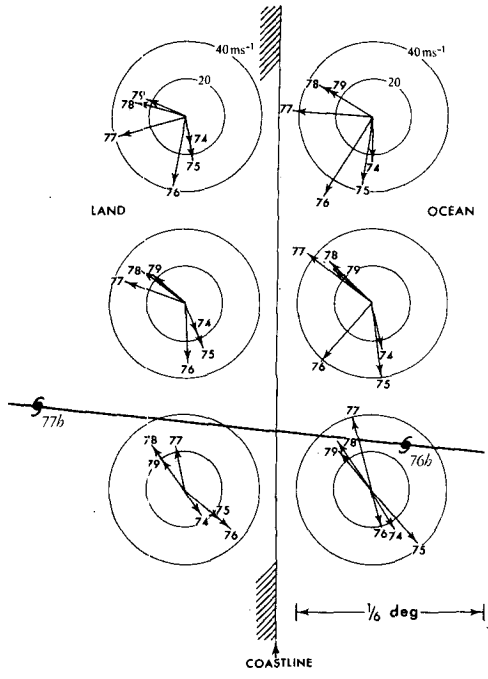

FIG. 3. Hourly low level ($\sigma = 0.992$) wind vectors at six grid points near the point of storm landfall for experiment L298 for the period 74–79 h. Storm track and 76 h and 77 h storm positions are also indicated. Land is to the west of the indicated coastline.

~180° change of wind direction and an initial reduction and subsequent increase of the wind speed upon passage of the storm center. At the grid points to the right and farther away from the storm track there is a more gradual veering of the wind from northerly to southeasterly, as one may expect from the influence of the steering current on the wind direction. Again notice the overall reduction of the wind speed over the land compared to that over the ocean.

c. *Precipitation analyses*

The precipitation rates for the basic landfall experiment L298 are analyzed for the same four time levels as the low-level wind field (Fig. 4). Before and during landfall, maximum rainfall rates exceed 7.2 cm h^{-1}. (The rates are for one model time step expressed in cm h^{-1}.) These maximum rates are associated with convective scale cells which move cyclonically around the storm center. They are imbedded in a larger storm scale rain area whose precipitation rate is 0.72–2.88 cm h^{-1}. A small increase in the average precipitation rate in the storm occurs near landfall relative to the ocean-only experiment. Two hours subsequent to landfall, the area of heavy precipitation (i.e., >2.88 cm h^{-1}) decreases as the storm decays. These rainfall rates and the areal coverage of these specific rates are comparable with those estimated over land by Parrish *et al.* (1982) for Frederic. Parrish *et al.* (1982) found a 50% increase in the areal coverage of mesoscale convection as Frederic made landfall. However, in the present simulation experiment, such a large change is not found at landfall. It will be shown in Section 4 that the precipitation rate, storm total rainfall and the decay rate are dependent on the land conditions specified.

d. *Moisture and kinetic energy budgets*

Moisture and kinetic energy budgets are analyzed for a 3.5 × 3.5° domain centered on and moving with the storm for the period 64–92 h. The equation describing the change of precipitable water can be written as

$$\overline{\frac{\partial}{\partial t}\int p_* r \frac{d\sigma}{g}} = -\overline{\int \nabla\cdot[(\mathbf{V}-\mathbf{C})p_* r]\frac{d\sigma}{g}} + \overline{\mathrm{EVAP}} - \overline{\mathrm{PREC}} + \overline{\mathrm{HDIF}}, \quad (3.1)$$

where the overbar denotes an area average, p_* the surface pressure, σ the sigma level (i.e., p/p_*), $\mathbf{V}$ the vector wind, $\mathbf{C}$ the mean storm movement vector, EVAP the evaporation rate, PREC the precipitation rate and HDIF the convergence of precipitable water into the storm area due to subgrid scale horizontal eddies. The term on the left-hand side of (3.1)

$$\int p_* r \frac{d\sigma}{g}$$

is the precipitable water and the first term on the right-hand side is the relative flux convergence of precipitable water into the storm area. In the calculations, $\mathbf{C}$ was taken as a constant value of 10.7 m s^{-1} westward, 1.4 m s^{-1} northward. Fig. 5 displays a complete moisture budget for experiment L298. The precipitation rate and the precipitable water of the ocean only control case are also shown for comparison purposes. After the increase of precipitation at landfall, relative to the ocean control case, the average precipitation of L298 decreases. At 89 h, the average precipitation rate is ~0.6 that of the ocean control case. As expected, there is a high correlation between the precipitation rate and flux convergence of moisture throughout the simulation. Balance of the moisture field is maintained before and for the first few hours after landfall by the relatively small evaporation term as well as by precipitation and moisture convergence. By three hours after landfall the evaporation is reduced to nearly zero because of the cool land surface temperature despite the moist land condition. As stated in TK, the reduction or elimination of evaporation has a subtle but vital effect on the moisture budget and subsequent decay of a tropical cyclone.

The kinetic energy budget for the moving storm domain is presented in Fig. 6 for L298. The kinetic energy equation can be written in the form

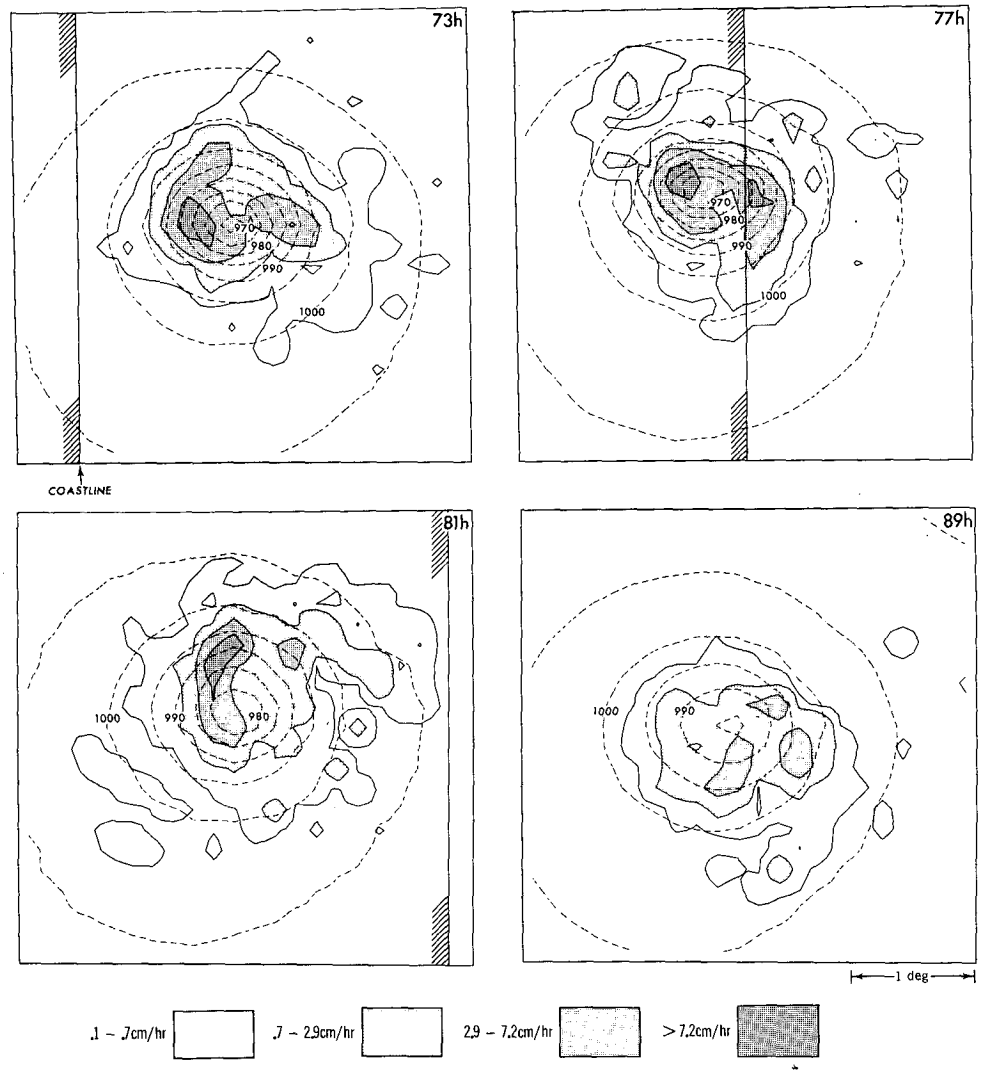

FIG. 4. Analyses of rainfall rates for the basic landfall experiment, L298, for 73, 77, 81 and 89 h. The shading legend indicates intensity in cm h^{-1}. The dashed lines are the isobars (mb) of the surface pressure field. Land is to the west of the indicated coastline.

$$\overline{\frac{\partial}{\partial t}\int p_*\left(\frac{u^2+v^2}{2}\right)\frac{d\sigma}{g}} = -\overline{\int \nabla\cdot\left[(\mathbf{V}-\mathbf{C})p_*\left(\frac{u^2+v^2}{2}\right)\right]\frac{d\sigma}{g}} - \overline{\int \mathbf{p}_*\mathbf{V}\cdot\nabla_p\phi\,\frac{d\sigma}{g}} + \overline{\int p_*\mathbf{V}\cdot\mathbf{F}_V\,\frac{d\sigma}{g}}, \quad (3.2)$$

where the overbar denotes the storm area average, u and v the zonal and meridional components of the wind, $\nabla_p\phi$ the geopotential gradient on a pressure surface, and $\mathbf{F}_V$ the frictional force. The quantity

$$\int p_*\left(\frac{u^2+v^2}{2}\right)\frac{d\sigma}{g}$$

is the vertical integral of the kinetic energy per unit area, the first term on the right-hand side is the relative flux convergence of kinetic energy per unit area,

$$-\int p_*\mathbf{V}\cdot\nabla_p\phi\,\frac{d\sigma}{g}$$

is the vertical integral of the generation of kinetic energy or the work done by the horizontal pressure gradient force per unit area, and

$$\int p_*\mathbf{V}\cdot\mathbf{F}_V\,\frac{d\sigma}{g}$$

is the vertically integrated dissipation of kinetic energy per unit area.

For comparison purposes, the kinetic energy and its generation are also shown for the ocean only control

case in Fig. 6. Up to a few hours after landfall the total kinetic energy is maintained by the balance between the generation, dissipation and flux divergence of kinetic energy. Relative to the control case the generation peaks at landfall, then together with the dissipation decreases for the rest of the experiment. After landfall the generation and dissipation terms approximately balance, while the flux divergence of kinetic energy remains relatively constant. The net result is a decrease in kinetic energy of the storm system as the tropical cyclone fills over land. It is found that the storm-average kinetic energy decreases by 20% from landfall to 14 h afterward, while the kinetic energy associated with the maximum low level winds decreases by 76%. This is because the inner storm area maximum winds are decreased more than the outer storm area winds and also because the boundary layer winds are reduced substantially more than the winds aloft.

In the primary experiment, the increase of both the kinetic energy generation and precipitation at and after landfall is less pronounced than that in TK, and in another experiment, L302, both in which the land surface temperatures were warmer (i.e., 302 K). This point will be discussed later in Section 4a.

4. Effect of different land surface conditions on tropical cyclone filling

An experiment was performed in which the LST was specified to a higher value (302 K) than in experiment L298 (298 K). In addition an experiment was performed in which a horizontally nonuniform z_0 instead of a constant value z_0 was specified over land. These experiments describe the sensitivity of the landfalling decay process to these presumably secondary physical effects.

a. Land surface temperatures

In order to study the impact of land surface temperature on landfalling storms, an experiment is performed in which the LST is specified as 302 K, the

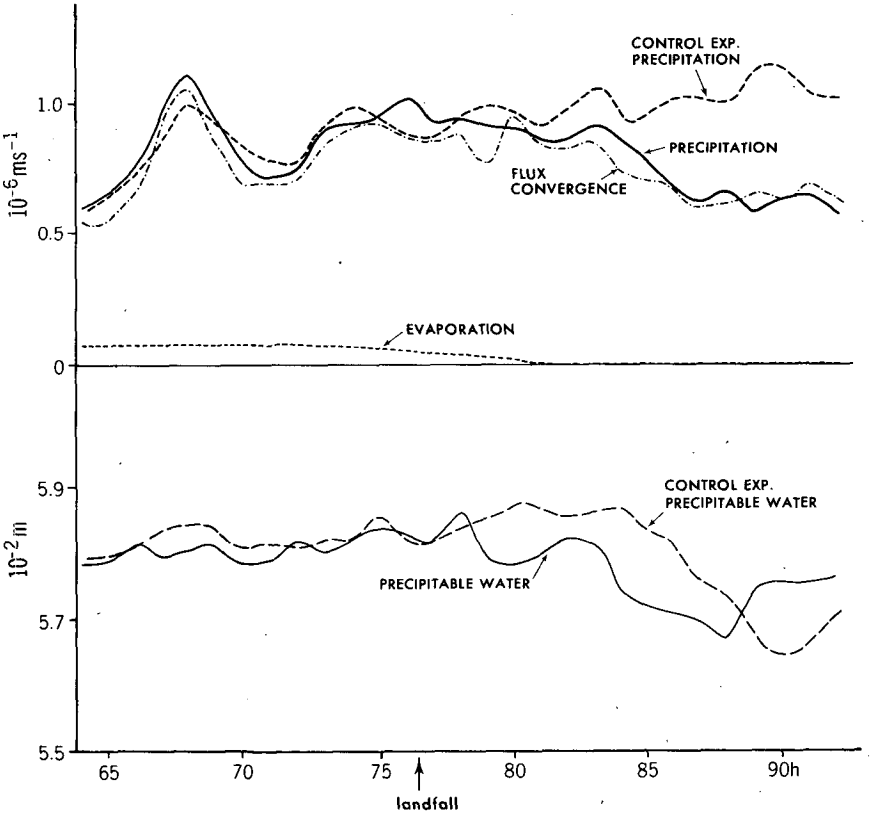

FIG. 5. Moisture budget for experiment L298 for the 3.5 × 3.5° domain relative to the moving storm. Also plotted (dashed lines) are the precipitation rate and the precipitable water for the ocean-only control experiment. The precipitation rate, expressed in 10^{-6} m s^{-1}, a negative component in the atmospheric moisture budget, is plotted as a positive term for comparison purposes. It may be converted to cm h^{-1} by multiplying by 0.36. The convergence due to subgrid scale horizontal eddies, HDIF in (3.1), is too small to be plotted. All quantities are calculated hourly; high frequency variations may not be accurately represented.

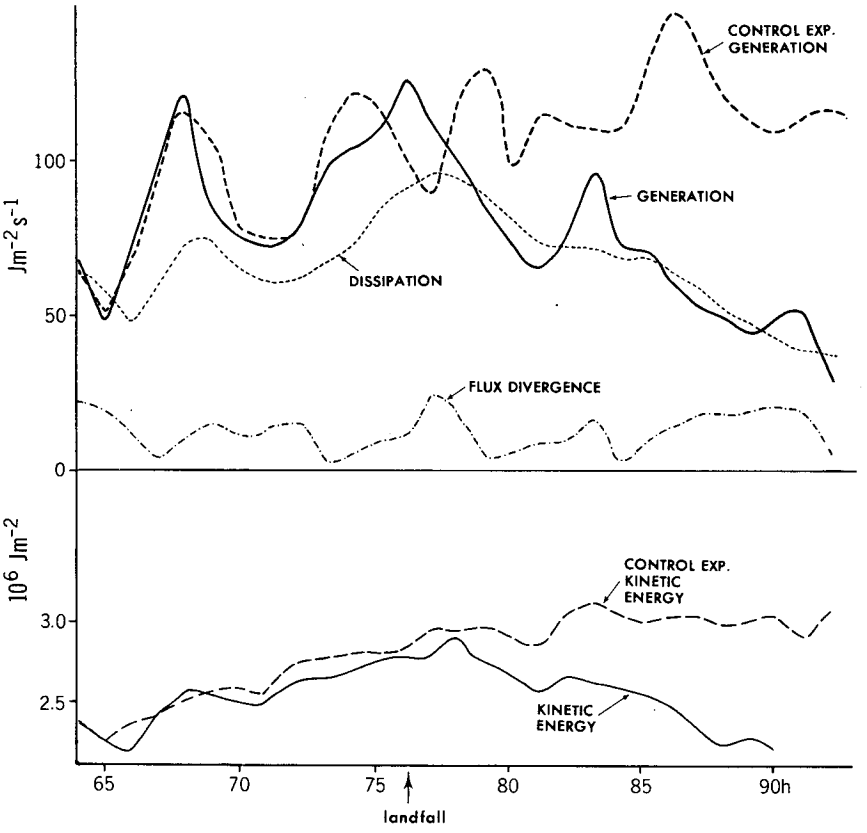

FIG. 6. Kinetic energy budget for experiment L298 for the 3.5 × 3.5° domain relative to the moving storm. The kinetic energy and generation of kinetic energy for the ocean control experiment are also shown for comparison purposes. The dissipation and flux divergence of kinetic energy, negative components in the atmospheric energy budget, are plotted with their signs reversed. All quantities are calculated hourly; high frequency variations may not be accurately represented.

same as the ocean temperature. In experiment L302, w is set to 0.0 so that there is no evaporation over the land. The surface roughness parameter is fixed at $z_0 = 25$ cm, the same as the basic landfall experiment. In L302 the storm fills significantly slower in the first 12 h than that in L298. For the warm LST case of experiment L302, hurricane force, low level winds penetrate ~403 km inland compared to 165 km for L298. The storm of L302 remains a hurricane for six more hours with low-level wind differences between the two storms exceeding 5 m s^{-1} for several hours after landfall (Fig. 7). The LST sensitivity in these two simulations is also apparent in the precipitation field. The average precipitation rate within the storm increases relative to the ocean control case in experiment L302 from 3 h before landfall to 10 h after landfall. At 81 h the storm-average (3.5 × 3.5° domain) precipitation rate is 1.19×10^{-6} m s^{-1} (0.43 cm h^{-1}) for L302 and 0.89×10^{-6} m s^{-1} (0.32 cm h^{-1}) for the ocean control case. This contrasts with the basic landfall experiment L298 in which the storm-average precipitation rate is 0.86×10^{-6} m s^{-1} (0.31 cm h^{-1}), already below that of the ocean control case. The contrast between experiments L298 and L302 can be seen also in the distribution of total rainfall during the storm passage (Fig. 8). The total rainfall along and near the storm track is significantly greater with warm LST, although the maximum total rainfalls observed are 20.4 and 19.6 cm in L298 and L302, respectively. These figures compare favorably with maximum totals for Frederic of 22.6 (radar) and 27.9 cm (gauge) as reported by Parrish *et al.* (1982) and Hebert (1980), respectively. Brunt (1968) has reported a range of 24 h maximum rainfall from 13 to 65 cm for 20 landfalling Australian cyclones. The extension of the 10 cm isopleth further to the right of the track than to the left at the point of landfall is also similar to the observation. In both model simulations, areas of heaviest rainfall occur to the right of the storm track 50 km inland. This probably can be related to the enhancement at the coastline of heavy precipitation cells such as those in Fig. 4 moving cyclonically around the storm center. Heavy total rainfall is due in part to these convective scale cells and their relative position and motion as shown by Parrish *et al.* (1982). The irregular nature of these cells result in a sporadic pattern of heavy

precipitation areas even in the ocean only control case. The intense cells situated to the left of the propagating storm (Fig. 4, lower right) move slower than those on the right side, relative to a fixed geographical point. As shown in Fig. 8 this results in rainfall totals exceeding 15 cm at certain areas to the left of the track even at distances greater than 400 km inland.

The intensity and total precipitation differences between low and high LST experiments can be related to the decrease of conditional instability over the cool land and the alteration of the bounday layer inflow. As shown by Fig. 9, saturated equivalent potential temperatures exceeding 360 K are quite limited over the land in experiment L298. Compared to L302, the lower tropospheric region in front of the storm near the coastline is more stable from the ground to above 800 mb. Miller (1964) observed surface equivalent potential temperature differences of 21 K between a hurricane over ocean and over land. As shown by TK, because of the increased surface roughness over land, the hurricane boundary layer tends to deepen with a corresponding increased radial inflow provided that the boundary layer stability remains the same (TK, Fig. 5). However, if the boundary layer becomes more stable, which occurs with cool land surface conditions, vertical mixing is suppressed and the increase of boundary layer radial inflow becomes less pronounced. For example, the average radial inflow at level 9 (~435 m) for four points 0.83 deg from the storm center is found to be 12.1, 9.1 and 6.2 m s^{-1} at 83 h for experiments L302, L298 and the ocean control case, respectively. In L298 these two factors (i.e., the decrease of conditional instability and alteration of the boundary layer inflow) contribute to the reduction of cross-isobaric flow, the resultant decrease of generation of kinetic energy and the decrease of the overall precipitation rate as compared with L302. This results in the increase of the decay rate of the storm provided that the surface evaporation is effectively retarded upon landfall.

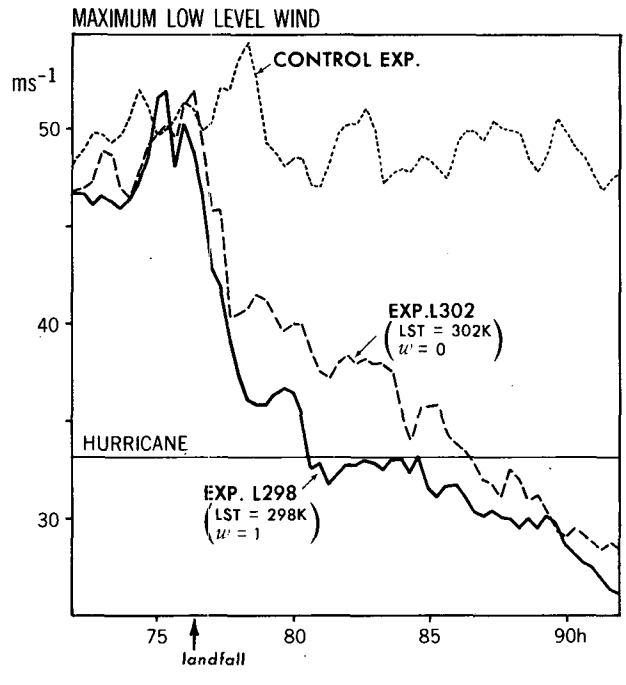

FIG. 7. The maximum low level (σ = 0.992) wind (m s^{-1}) as a function of time for experiments L302, L298 and the ocean-only control experiment, LST refers to the specified land surface temperature and w refers to the moisture availability of the land surface as used in (2.2).

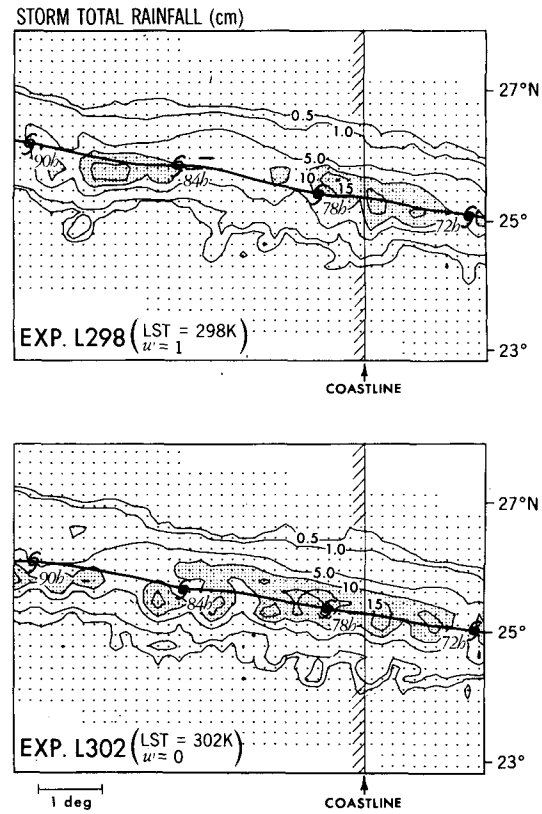

FIG. 8. Storm total rainfall (cm) for experiment L298 (top) and L302 (bottom). The storm tracks with 6 h positions are also shown for the two experiments. Total rainfall greater than 10 cm is shaded; LST and w refer to specified land surface temperature and moisture availability respectively. Land is to the west of the indicated coastline and the dots indicate the fine mesh resolution of ~17 km at 25°N.

b. *Effect of variable surface roughness*

Since surface roughness over land can be quite variable in reality, the sensitivity of the landfall simulation to the roughness distribution is tested by introducing a horizontally variable land roughness. The dashed lines of Fig. 10 describe the roughness field which is varied from z_0 = 10 cm at the coast to a maximum of z_0 = 100 cm centered 1.5° from the coast directly in the storm's path. Except for the roughness parameter

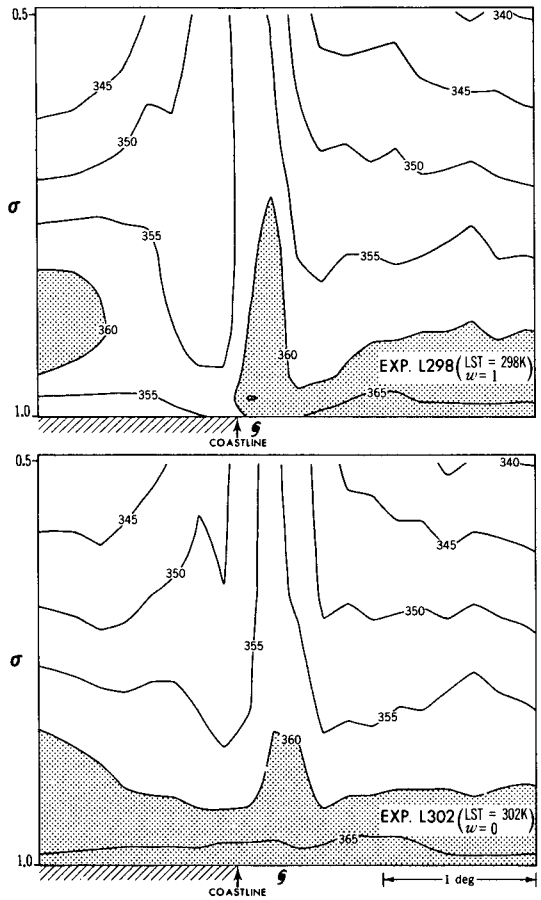

FIG. 9. East–west cross section of saturated equivalent potential temperature (K) through the storm center within an hour of landfall (76 h) for experiments L298 and L302. The analyses are for the lower half of the model atmosphere, $\sigma \geq 0.5$, with values greater than 360 K shaded; LST and w refer to specified land surface temperature and moisture availability, respectively. Land is to the west of the indicated coastline.

z_0 the experiment, designated as V298, is identical to L298. The maximum, low-level wind swath shown in Fig. 10 indicates a decrease of ~5 m s^{-1} over the z_0 = 100 cm area compared to L298 (Fig. 1, upper part). Fig. 10 displays a rapid adjustment of the low-level wind field to the underlying surface roughness as can be seen by the kink of the isotachs at each discontinuity of roughness length. Although not shown, a small change also occurs in the upper level wind field and surface central pressure (~3 mb increase) while the storm is over the rough land area, but the storm quickly recovers to the same intensity as in L298 by 90 h after moving back over the relatively smooth surface. No large differences in the storm total rainfall amounts are evident near the rough anomaly. Perhaps the storm system sensitivity to z_0 would be more acute if the anomaly was specified closer to the coastline. The effect of topography on landfalling tropical cyclones may have a bigger impact than roughness variability, especially in mountainous areas (e.g., Chang, 1982).

5. Effect of storm intensity on filling rates at landfall

Observed tropical cyclones make landfall at a variety of intensities. In order to study the behavior of a smaller, less intense storm at landfall, another experiment is performed. The decay rate of this experiment and the other previous experiments will be compared to the observed fill rates of 11 hurricanes.

a. A small, less intense storm at landfall

The simulation studies described to this point have all been of moderate size storms with 30 m s^{-1} winds extending out ~75 km from the center and with central pressures between 960 and 965 mb before landfall. In experiment S302, R_m and R_0 in (2.3) are specified to be 150 and 1167 km, respectively, LST = 302 K, z_0 = 25 cm, and w = 0.0. All other parameters including the basic flow are identical to the other landfalling experiments. The vortex is then spun up to hurricane strength in analogous fashion to the other experiments. The differences in the initial conditions for the vortex result in a smaller, less intense storm upon reaching its approximate steady state. The central pressure 3 h before landfall is 979 mb with 30 m s^{-1} winds extending out 63 km from the center. For comparison purposes, Table 3 displays some of the basic indicators of the size and strength of the tropical cyclones of this study and that of TK ~3 h before landfall. As shown in Fig. 11, there is a rapid decrease in the low-level winds immediately upon landfall in S302. In less than 2 hours after landfall, the low-level winds are below hurricane

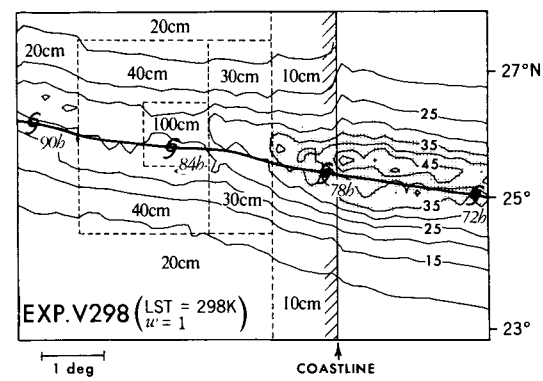

FIG. 10. Horizontal distribution of maximum low level (σ = 0.992) wind (m s^{-1}) during the tropical storm passage for experiment V298. Dashed lines over land indicate the horizontal variation of the roughness parameter z_0 (cm). Shading indicates hurricane force winds. The storm track with 6 h storm position is also indicated; LST and w refer to specified land surface temperature and moisture availability, respectively. Land is located to the west of the indicated coastline.

TABLE 3. Some basic indicators of size and strength of the tropical cyclones of this study and that of Tuleya and Kurihara, 1978: p_{min}, central surface pressure; $|V_{max}|$, maximum low level ($\sigma = 0.992$) wind speed; R_{max}, the distance north from the location of p_{min} to that of the strongest wind; and R_{30} and R_{20}, the distance north from the location of p_{min} to that of the outer 30 and 20 m s^{-1} contour, respectively. Values indicated are those for ~3 h prior to landfall. Note that in TK, no explicit basic flow was included: this will affect the values of $|V_{max}|$, R_{max}, R_{30}, and R_{20}.

Experiment	p_{min} (mb)	$\|V_{max}\|$ (m s^{-1})	R_{max} (km)	R_{30} (km)	R_{20} (km)
Control	966	50	33	89	167
L298	967	47	33	91	169
L302	969	49	32	89	169
V298	966	47	33	93	174
S302	979	40	33	63	139
TK	966	40	52	96	168

force. After this time, they decrease very slowly. In fact at 15 h after landfall the low level winds of the small storm in experiment S302 and its large counterpart in L302 are comparable. Nineteen hours after landfall the central surface pressure of the large and small storms are within 3 mb of each other (985 and 988 mb). The 12 h fill rate for the small storm is only 9 mb, while that for the large storm is 16 mb. It was mentioned in Section 4 that for a moist, cool land surface, i.e., LST = 298 K and $w = 1.0$, the large storm decayed even more quickly. The fill rate of the storm in L298 is 20 mb for the first 12 h after landfall.

b. Comparison of fill rate with observation

The simulation studies performed here are still quite idealized, and rather arbitrary assumptions are made. Despite these reservations, it is appropriate to study and compare the decay rates for the present study with those observed for individual Atlantic and Gulf storms for 1969–79. The fill rates were determined from National Hurricane Center yearly summaries (e.g., Simpson *et al.*, 1970). Fig. 12 displays the fill rate as a function of the central surface pressure at landfall. One immediately sees the positive relationship between intensity and fill rate. The stronger hurricanes, e.g., Camille in 1969, fill more rapidly than the weak storms. The 12 h fill rates of the observed storms range from 2 mb (Babe, 1977) to 73 mb (Camille, 1969). A similar pattern can be derived for 24 landfalling hurricanes (1928–77) from the data set of Jarvinen and Caso (1978).[2] The experimental data of the present simulations, experiments S302, L302, V298 and L298, are also plotted as well as that of the experiment of TK. It is encouraging that, for the same landfalling intensity, the 12 h fill rates of the model storms are quite similar to the observed ones. In addition, the same relationship is found between intensity and fill rate of the model storms as those of the observations although it is over a much smaller intensity range. It appears that the basic early 12 h decay rate can be adequately treated using the present experimental design although fluctuations of other conditions may enhance or retard the decay process. After 12 h it is speculated that other factors such as the influence of continental air masses and frontal interactions will have an increasing influence.

6. Remarks and conclusions

Under a rather idealized experimental framework, the present series of landfalling experiments produced realistic results. Model filling rates ranged from 9 to 20 mb per 12 h which correspond well to observed filling rates for comparable storm intensity. Also as in observation, the filling rate was shown to be a function of storm intensity. Synoptic features of the wind and precipitation field also appeared quite reasonable and often agreed with the limited observations. The low-level maximum wind field was changed sharply at the coastline and rapidly decayed inland. The precipitation pattern was found to be a complex phenomena, dependent on the response of the naturally occurring convective scale cells to the changes of the surface conditions at and after landfall. The energy and mois-

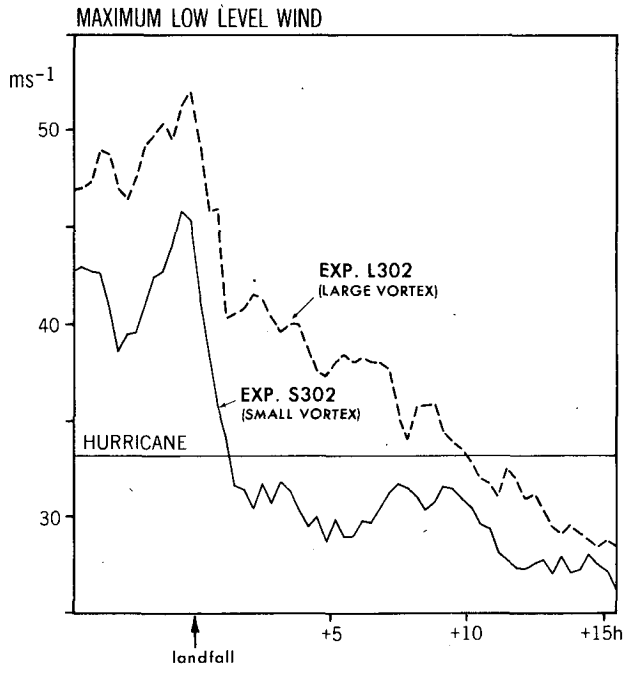

FIG. 11. The maximum low level ($\sigma = 0.992$) wind (m s^{-1}) as a function of time for experiment L302, a large model storm, and S302, a small model storm. L302 was initialized with $R_m = 200$ km and $R_0 = \infty$ in (2.3). S302 was initialized with $R_m = 150$ km and $R_\infty = 1167$ km in (2.3).

[2] Data supplied by personal communication with P. N. Georgiou of the University of Western Ontario.

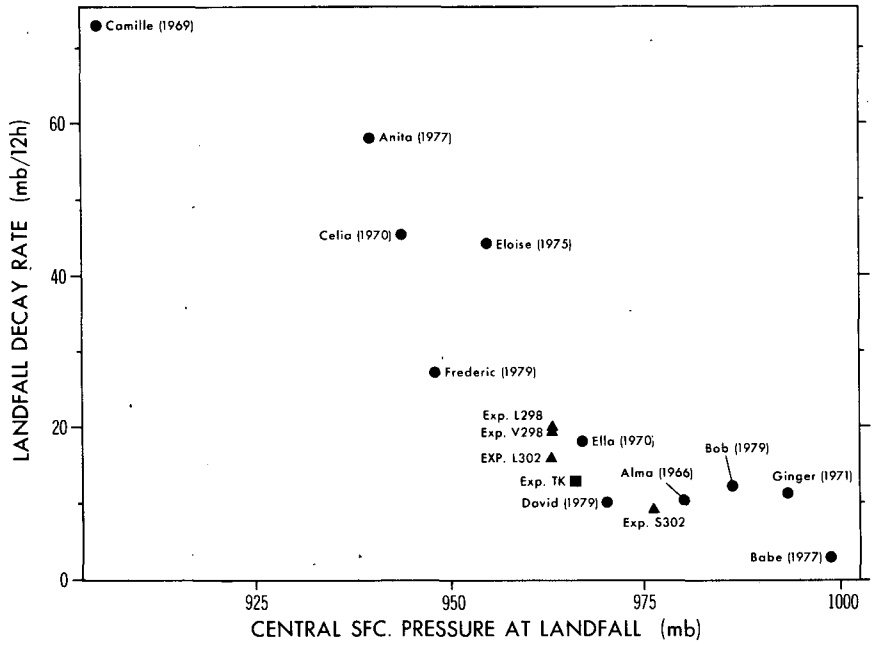

FIG. 12. Twelve hour fill rate as a function of the central surface pressure at the time of landfall for 11 observed hurricanes of the Gulf and Atlantic. Data for model landfall simulations experiments L298, S302, L302, V298 in addition to the landfall experiment of Tuleya and Kurihara (1978) are also shown.

ture budgets for the storm area revealed a high correlation between the decay of the storm and the decrease of evaporation, precipitation and energy generation beginning several hours after landfall.

Previous studies have demonstrated the principal role of the retardation of evaporation in the landfall decay process. It was found in this study that the landfall decay process can be modified by the surface land conditions which are specified. The evolution of the wind and pressure fields and the rainfall distribution were significantly changed by different land surface conditions. A cool land enhanced the decay through a decrease in conditional instability and an alteration in the depth and strength of the planetary boundary layer inflow. This was especially true in the first 12 h after landfall. Inhomogeneity of surface roughness caused observable changes in the pressure and wind field near the location of large surface roughness anomalies, but the overall decay process did not seem to be permanently affected.

It is encouraging that the results simulated observed landfall reasonably well. One factor in the decay process not considered is the effect of topographical features which could have significant impact on the decay of a landfalling storm. Also, the effects of the speed, direction and nonuniformity of the steering current, a subsequent interaction with an adjoining air mass, and a transformation into an extratropical system as well as the effects caused by temporal and spatial variations in surface temperature and moisture have been excluded. In the present study, these simplifications had the advantage in isolating the basic landfalling process. However, these subjects need to be considered in future research.

Acknowledgments. The authors would like to express their appreciation to J. Smagorinsky for his constant support of the hurricane dynamics project during his directorship of the Geophysical Fluid Dynamics Laboratory. They wish to thank J. Mahlman of GFDL and R. Burpee, M. Powell and other colleagues of theirs at the Atlantic Oceanographic and Meteorological Laboratory for constructive comments and criticisms on a preliminary version of this manuscript. They also acknowledge the useful comments by the reviewers on the original version of this paper. P. Tunison, W. Ellis, M. Zadworny, K. Raphael, J. Conner and J. Kennedy deserve credit for assistance in the preparation of this manuscript.

REFERENCES

Anthes, R. A., 1982: *Tropical Cyclones. Their Evolution, Structure and Effects. Meteor. Monogr.* No. 41, Amer. Meteor. Soc., 208 pp. [ISBM 0-933876-54-8].

Brunt, A. T., 1968: Space-time relations of cyclone rainfall in the northeast Australian region. *Civil Eng. Trans. Inst. Eng. Australia,* April issue, 40–46.

Chang, S. W., 1982: The orographic effects induced by an island mountain range on propagating tropical cyclones. *Mon. Wea. Rev.,* **110,** 1255–1270.

Fujita, T. T., 1980: In search of mesoscale wind fields in landfalling hurricanes. *Proc. 13th Tech. Conf. on Hurricanes and Tropical Meteor.*, Miami Beach, Amer. Meteor. Soc., 43–57.

Hebert, P. J., 1980: Atlantic hurricane season of 1979. *Mon. Wea. Rev.*, **108,** 973–990.

Hubert, L., 1955: Frictional filling of hurricanes. *Bull. Amer. Meteor. Soc.*, **36,** 440–445.

Jarvinen, B. R., and E. L. Caso, 1978: A tropical cyclone data tape for the North Atlantic basin, 1886–1977: Contents, limitations, and uses. NOAA Tech. Memo. NWS NHC6, NOAA/NWS/NHC, Miami, 1–19.

Kurihara, Y., 1973: A scheme of moist convective adjustment. *Mon. Wea. Rev.*, **101,** 547–553.

——, and M. A. Bender, 1980: Use of a movable nested-mesh model for tracking a small vortex. *Mon. Wea. Rev.*, **108,** 1792–1809.

——, and ——, 1982: Structure and analysis of the eye of a numerically simulated tropical cyclone. *J. Meteor. Soc. Japan,* **60,** 381–395.

—— and ——, 1983: A numerical scheme to treat the open lateral boundary of a limited area model. *Mon. Wea. Rev.*, **111,** 445–454.

——, and R. E. Tuleya, 1974: Structure of a tropical cyclone developed in a three-dimensional numerical simulation model. *J. Atmos. Sci.*, **31,** 893–919.

Mellor, G. L., and T. Yamada, 1974: A hierarchy of turbulence closure models for planetary boundary layers. *J. Atmos. Sci.*, **31,** 571–583.

Miller, B., 1964: A study of the filling of hurricane Donna (1960) over land. *Mon. Wea. Rev.*, **92,** 389–406.

Moss, M. S., and R. W. Jones, 1978: A numerical simulation of hurricane landfall. NOAA Tech. Memo. ERL NHEML-3, NOAA/AOML/HRD, Boulder, 1–15.

Parrish, J. R., R. W. Burpee, F. D. Marks, Jr. and R. Grebe, 1982: Rainfall patterns observed by digitized radar during the landfall of hurricane Frederic (1979). *Mon. Wea. Rev.*, **110,** 1933–1944.

Powell, M. D., 1982: The transition of the hurricane Frederic boundary wind field from the open Gulf of Mexico to landfall. *Mon. Wea. Rev.*, **110,** 1912–1932.

Shea, D. J., and W. M. Gray, 1973: The hurricane's inner core region. I: Symmetric and asymmetric structure. *J. Atmos. Sci.*, **30,** 1544–1564.

Simpson, R. H., and H. Riehl, 1981: *The Hurricane and its Impact.* Louisiana State University Press, 398 pp. [ISBM 0-8071-0688-7]

——, A. L. Sugg and staff, 1970: The Atlantic hurricane season of 1969. *Mon. Wea. Rev.*, **98,** 293–306.

Tuleya, R. E., and Y. Kurihara, 1978: A numerical simulation of the landfall of tropical cyclones. *J. Atmos. Sci.*, **35,** 242–257.